Desalination and Water Treatment
www.deswater.com

doi: 10.5004/dwt.2021.26517

210 (2021) 240–249
January

Zeolitic imidazole framework (ZIF) – zinc oxide nanocomposite: synthesis and ultrasound-assisted pollutant removal from the binary system

Atefeh Panahdar[a,b], Sepideh Langari[a], Niyaz Mohammad Mahmoodi[a,*], Samira Ghiyasi[b], Mohammad Reza Saeb[c], Kumars Seifpanahi-Shabani[d], Mojtaba Jalili[e]

[a]*Department of Environmental Research, Institute for Color Science and Technology, Tehran, Iran, Tel. +98 21 22969771; Fax: +98 21 22947537; emails: mahmoodi@icrc.ac.ir/nm_mahmoodi@aut.ac.ir (N.M. Mahmoodi), atefe.panahdar90@gmail.com (A. Panahdar), langari.sepideh@gmail.com (S. Langari)*
[b]*Department of Environmental Engineering, Central Tehran Branch, Islamic Azad University, Tehran, Iran, email: s.ghiasi@iautctb.ac.ir*
[c]*Department of Resin and Additives, Institute for Color Science and Technology, Tehran, Iran, email: mrsaeb2008@gmail.com*
[d]*Faculty of Mining, Petroleum and Geophysics Engineering, Shahrood University of Technology, Shahrood, Iran, email: seifpanahi@shahroodut.ac.ir*
[e]*Department of Printing Ink Science and Technology, Institute for Color Science and Technology, Tehran, Iran, email: Jalili@icrc.ac.ir*

Received 25 February 2020; Accepted 28 August 2020

ABSTRACT

Nowadays, the overuse of dyes and their presence in wastewater can be considered as an environmental concern. In this study, zeolitic imidazole framework-8 (ZIF-8), zinc oxide (ZnO), and their composite (ZnO-ZIF-8) were synthesized and characterized by scanning electron microscopy, Fourier transform infrared, X-ray diffraction, and zeta potential techniques. The synthesized materials were used for the removal of Malachite green (MG) from aqueous media via a batch adsorption process. The adsorption isotherm, and the effects of operational parameters, including adsorbent dosage, initial dye concentration, time, and pH on dye removal, were comprehensively studied. The adsorption capacity of the composite was 3,654 mg/g. The results showed that the experimental data were fitted by the Freundlich isotherm model with a high correlation coefficient (0.9676). Moreover, the ability of the prepared adsorbents (ZIF-8, ZnO, and ZnO-ZIF-8) for the removal of dyes from binary systems containing MG and Rhodamine-B (Rh-B) was evaluated.

Keywords: Zeolitic imidazole framework (ZIF); Zinc oxide (ZnO); Composite (ZIF-ZnO); Pollutant removal; Binary system

1. Introduction

No one can deny the importance of nature and its cleanliness. With the industrial revolution and the significant growth of factories, a massive amount of industrial wastewater was discharged, causing many problems in the environment. One of the concerns was the overbalance in utilizing dyes in various industrial factories [1–3]. Therefore, wastewater treatment and removal of dyes have become a necessary strategy to reduce the adverse effects [4,5]. Different treatment techniques, such as adsorption, membrane, enzymatic, etc., have been utilized in wastewater treatment [6]. Due to the ease of operation and low economic cost, the adsorption process is one of the best

* Corresponding author.

methods for the removal of dyes [7–11]. Various adsorbents such as nanofibers, metal-organic frameworks (MOFs), etc. have been used to remove different dyes from wastewater [12,13]. The MOFs, as highly porous minerals, are promising candidates for the removal of dyes [14,15]. Zeolitic imidazole framework-8 (ZIF-8) is a MOF well-known class of family for highly effective wastewater treatment thanks to its very high surface area created by a super-porous structure [16–18]. Malachite green (MG) is a dye molecule widely used in the industry, and because of its complex structure, its removal process has always been recognized as a challenge [19,20]. MG has long-term effects with a very high toxic nature, causing eye irritation, headache, and heartbeat [21].

Various MOFs (such as ZIF-8) have been used in several studies for the removal of contaminants [22]. However, a zinc oxide (ZnO)-ZIF-8 composite has not been used to adsorb MG. Moreover, the importance of pH has not been studied in previous investigations, while pH plays a significant role in the process. As another critical factor, it was attempted here to apply sonication instead of stirring and shaking employed in previous studies. The isotherm of the adsorption process was also studied. The prepared nanoparticles were characterized by Fourier transform infrared (FT-IR), scanning electron microscopy (SEM), and zeta potential, and X-ray diffraction (XRD). The influence of different parameters (adsorbent dosage, initial dye concentration, time, and pH) on dye adsorption was also assessed.

2. Experimental

2.1. Materials

All chemicals used in this study were analytical grade. NaOH, $ZnCl_2$, $CuSO_4$, and $Zn(NO_3)_2{\cdot}6H_2O$ were purchased from Merck (Germany), and imidazole was obtained from Sigma-Aldrich (Germany). The MG was purchased from Ciba (Switzerland), and Rhodamine-B (Rh-B) was obtained from Samchun Pure Chemicals (Republic of Korea).

2.2. Synthesis of materials

NaOH (1 g) was dissolved in 90 mL of distilled water, and then $ZnCl_2$ (1 g) was added to the NaOH solution. The mixture was stirred for 30 min at room temperature. The solution was then heated for 24 h at 100°C. The liquid phase was removed, and the solid (ZnO) was washed and heated to dryness [23].

1.298 g of 2-methylimidazole (hmim) and 0.587 g of $Zn(NO_3)_2{\cdot}6H_2O$ were dissolved in 40 mL of methanol (MeOH). While the Zn^{2+} solution was being stirred, the hmim solution was added, and the mixture was stirred for 2 h at 25°C. Finally, the crystals (ZIF-8) were separated by centrifugation and washed with anhydrous ethanol, and dried at 60°C.

Overall, 0.587 g $Zn(NO_3)_2{\cdot}6H_2O$ and 0.4 g as-synthesized mesoporous ZnO were added in 40 mL of methanol and stirred for an hour. 1.298 g hmim was dissolved in 40 mL of methanol to achieve a clear solution. After that, it was mixed with the previous solution and placed on the stirrer at room temperature (theoretical mass ratio of ZIF-8 to ZnO was 1:2). Centrifugation was carried out several times, and the solid material (ZnO-ZIF-8) was washed with methanol and water. Afterward, it was dried at 60°C for 12 h.

3. Results and discussion

3.1. Characterization

An essential and useful tool for determining the porosity, shape, and size distribution of particles is SEM [24]. The morphology of the prepared ZnO, ZIF-8, and their composite (ZnO-ZIF-8) was examined using SEM, as shown in Fig. 2. It can be seen that the particles of ZIF-8 are compounded with ZnO.

The XRD pattern of as-prepared powder is shown in Fig. 3. The main diffraction peaks of ZIF-8 at around 2θ = 7°, 10°, 12°, 18°, 26°, and 29° can be seen in this pattern. These characteristic peaks indicate the formation of the ZIF-8 crystalline structure with high crystallinity, which is in agreement with previously reported literature [25]. The synthesized ZnO showed some sharp and intense peaks. The diffraction peaks of 31°, 34°, 36°, 47°, 56°, 62°, and 67° are related to (111), (002), (101), (102), (110), (103), and (102) facet of hexagonal wurtzite, respectively [26–28]. The high intensity of the mentioned peaks indicates the synthesized ZnO has crystallized well. The presence of those three intense characteristic peaks of 31°, 34°, and 36° confirms the presence of wurtzite aggregate. Hence, those appeared peaks in the range of 4°–20° are in the same

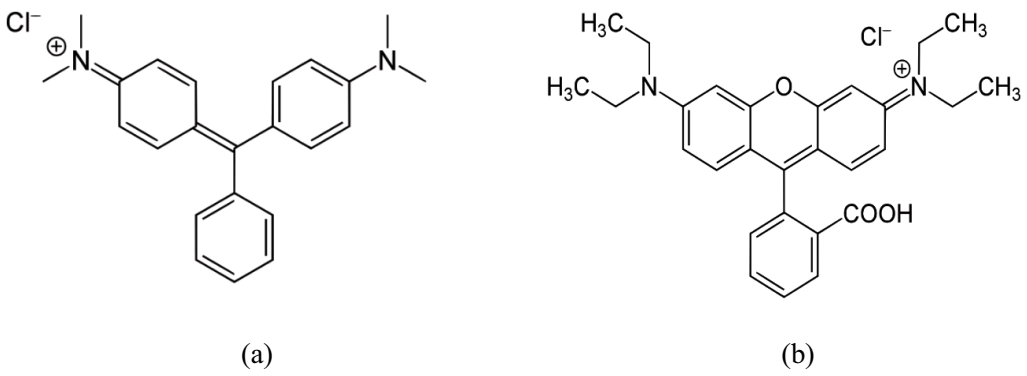

(a) (b)

Fig. 1. Structure of (a) MG and (b) Rh-B.

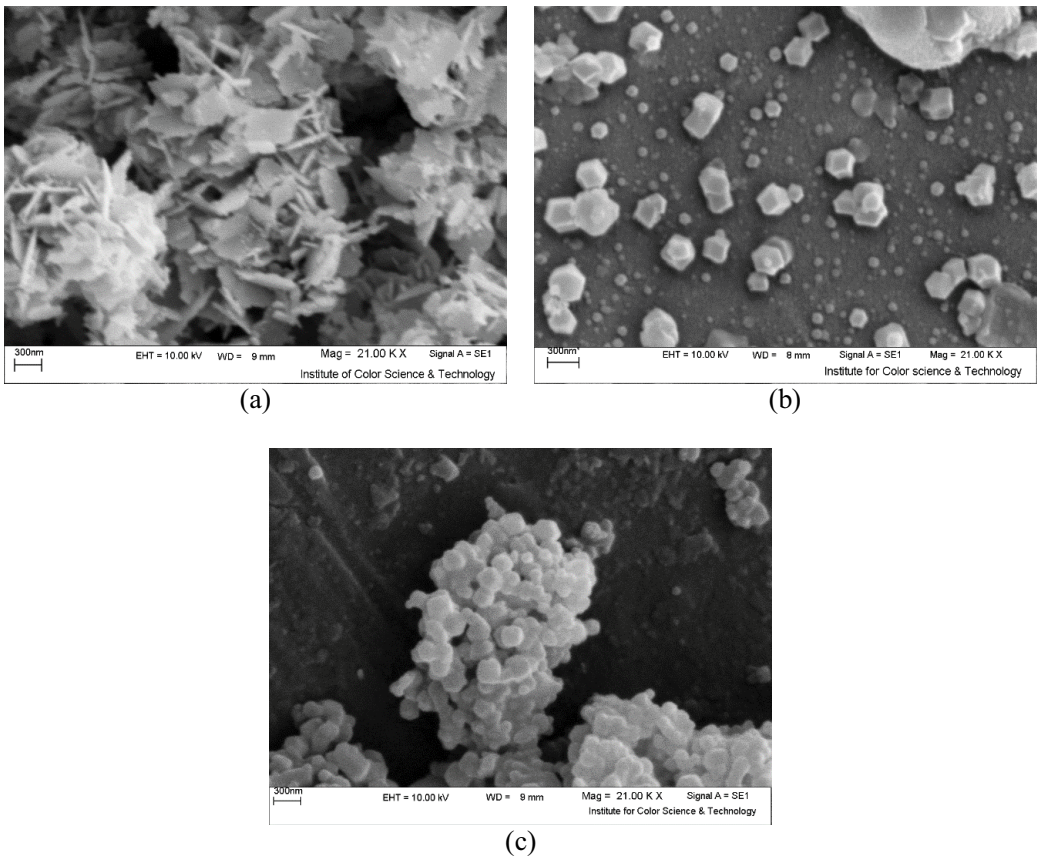

Fig. 2. SEM images (a) ZnO, (b) ZIF-8, and (c) ZnO-ZIF-8 composite.

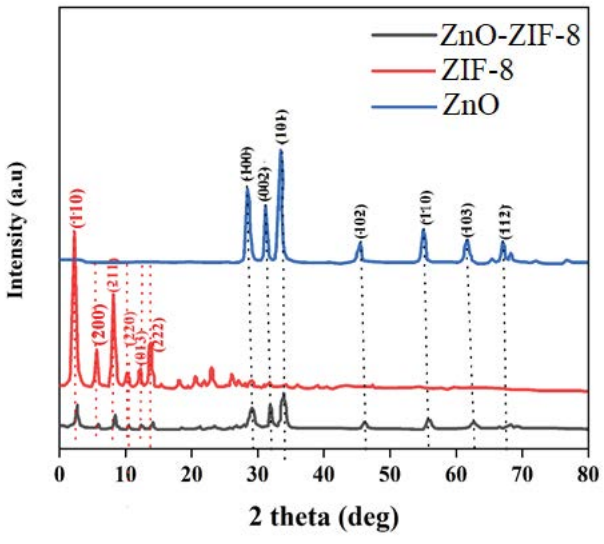

Fig. 3. XRD pattern of materials.

position to the comparison of single-phase ZIF-8 corroborate the growth of ZIF-8 on the ZnO beads [29]. No extra diffraction peak, which shows impurities, could be found in the composite. The significant intensity decrease of all peaks could be related to the partial coverage of ZnO beads by ZIF-8. Besides, this causes to pore-clogging of ZnO beads and some changes in the ZIF-8 particle size [26].

The characteristic bands of pure ZIF-8 in the range of 1,350–600 cm^{-1} (Fig. 4) are related to the in-plane bending modes of the imidazole ring [30–32], and the intense bands at the range of 1,500–1,350 cm^{-1} are assigned to stretching and vibration of the imidazole ring [33–35]. The band at 1,580 cm^{-1} indicates the imidazolic stretching vibration of C=N [36]. The peaks at 2,960 and 2,930 cm^{-1} are assigned to aliphatic C–H bond, related to the antisymmetric stretching vibration of CH_3 and CH_2 in the imidazole ring [35]. The aromatic C–H bond of the imidazole ring is significant at about 3,135 cm^{-1} [33,35]. The peak at 3,430 cm^{-1} can be attributed to the O–H bond and could be due to the presence of other hydroxylic groups at the ZIF-8 framework and chemisorbed water. A strong absorbance in the ZnO spectrum at around 480 cm^{-1} is related to the ZnO stretching vibration bond. Two intense peaks at 1,592 and 3,448 cm^{-1} correspond to the O–H bond and might be due to the adsorbed water and reaction of ZnO and other derivatives with oxygen [37,38]. The bands at around 600–1,500; 1,580; 2,960; 2,930; and 3,135 cm^{-1} in ZnO-ZIF-8 composite spectrum show the presence of imidazole rings of ZIF-8 in the composite. There are some peaks shifted and also slightly strengthened, suggesting a fine-ordering structure of the composite. Hence, the band at 480 cm^{-1} is attributed to the Zn–O bond, which confirms the presence of wurtzite in the composite.

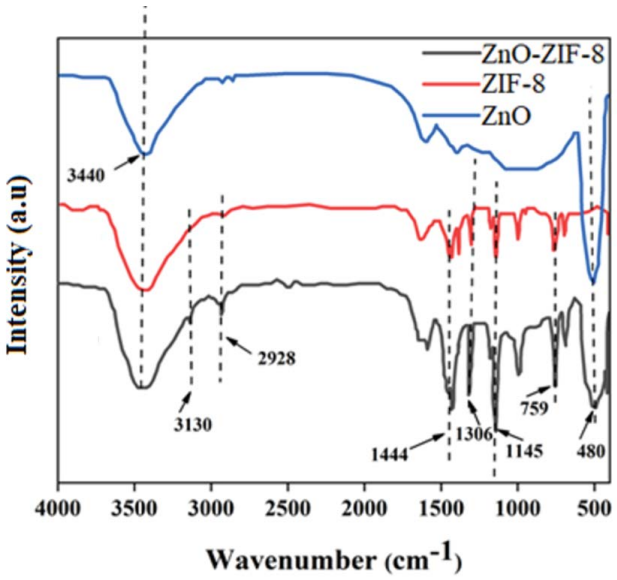

Fig. 4. FT-IR spectra of materials.

The zeta potential (Fig. 5) was measured by analyzing 0.004 g of ZnO, ZIF-8, and ZnO-ZIF-8 in 100 mL of water. Before zeta potential measurements, all samples were sonicated for 30 min. The pH of the samples was 6.5. The data indicate that the adsorbents have a negative surface charge, which is suitable for adsorption of cationic dye molecules.

3.2. Dye adsorption

3.2.1. Effect of adsorbent dosage

The amount of adsorbent is one of the most important factors in the adsorption process. This parameter is also momentous to estimate the cost of the adsorption process [39]. We used 100 mL of dye solution of MG with 50 mg/L concentration (initial) at room temperature for 30 min in pH 5 to investigate this parameter. An ultrasonic bath (30 kHz and power of 200 W) was used to assist dye removal. The percentage of dye removal assisted by ultrasound is higher than the assisted by stirring due to the considerably increasing mass transfer in the adsorption process [10].

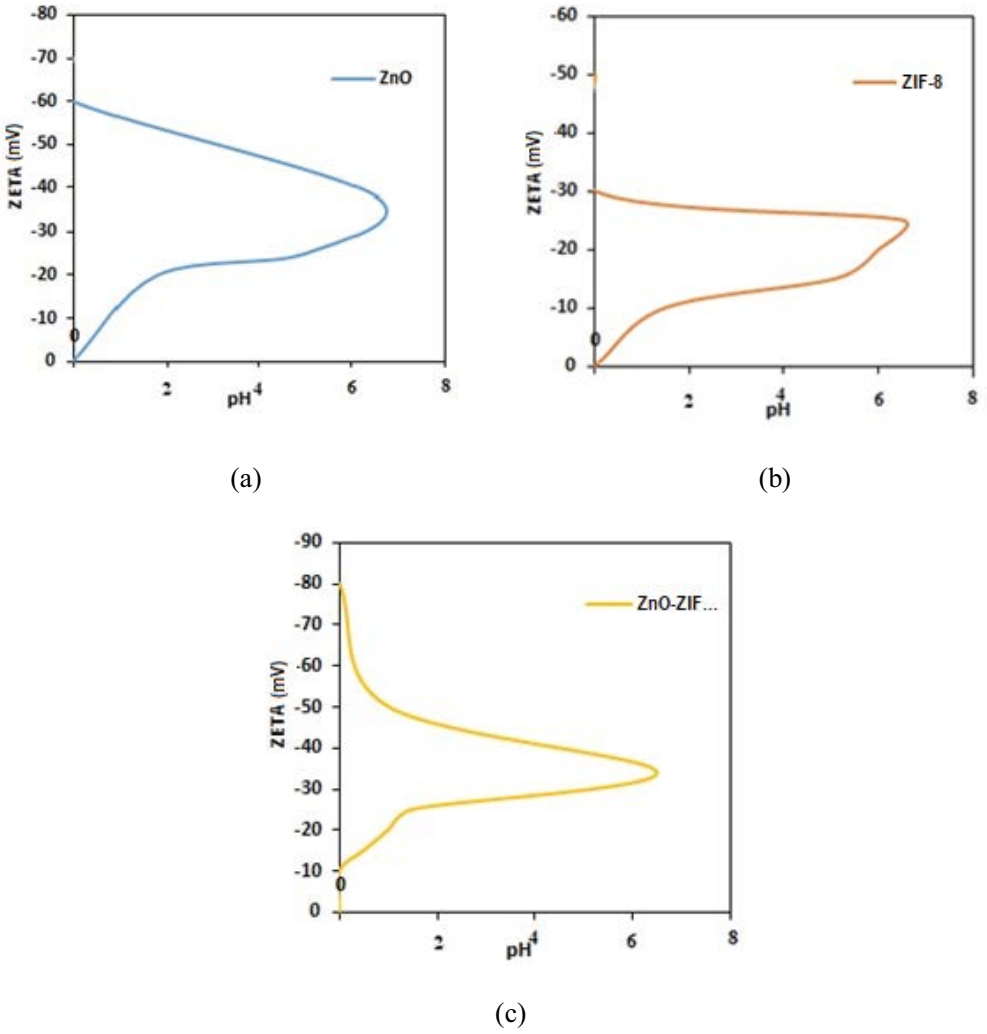

Fig. 5. Zeta potential graph of materials (a) ZnO, (b) ZIF-8, and (c) ZnO-ZIF-8.

Different adsorbent dosages (0.001, 0.002, 0.003, and 0.004 g) for MG solutions were used. Each experiment was sampled at specific time intervals. The samples were centrifuged, and the amount of dye in the supernatant was determined using a spectrophotometer. The charts of dye removal (%) vs. time at different adsorbent dosages are shown in Fig. 6 for three different adsorbents (ZnO, ZIF-8, and ZnO-ZIF-8). For all three adsorbents, increasing adsorbent dosage increases dye removal percent due to the increased availability of active adsorbent sites.

3.2.2. Effect of time

Another critical factor in the adsorption process is the contact time. In this article, the influence of this critical factor is investigated (contact time with different adsorbent doses, Fig. 6). As time increased, the dye removal percent increased. The active sites of the adsorbent decrease gradually during the adsorption process, and after a certain time, the adsorbent sites are no longer able to absorb more MG molecules. This time is called equilibrium time. Equilibrium time was 30 min in our experiments.

3.2.3. Effect of dye concentration

Another effective factor in dye removal that was investigated in our study was dye concentration. There is a direct relationship between the adsorption process and the initial dye concentration [37,39]. In this study, different concentrations of dye were investigated. As shown in Fig. 7, the adsorption rate decreases with increasing dye concentration, which is probably due to the saturation of active binding sites on the adsorbent surface at higher concentrations [40].

3.2.4. Effect of pH

The pH value is a very effective parameter because both the adsorbent and dye are affected by this parameter. The material surface charge and the adsorbate ionization degree is affected by this parameter [41]. Three different pH values (3.5, 6.5, and 8.5) were investigated (Fig. 8). The removal percentage of MG at different pH values is shown in Fig. 8 (pH 3.5: dye removal percentage for ZnO = 47%, ZIF-8 = 25%, and ZnO-ZIF-8 = 75%), (pH 6.5: dye removal percentage for ZnO = 62%, ZIF-8 = 55%, and

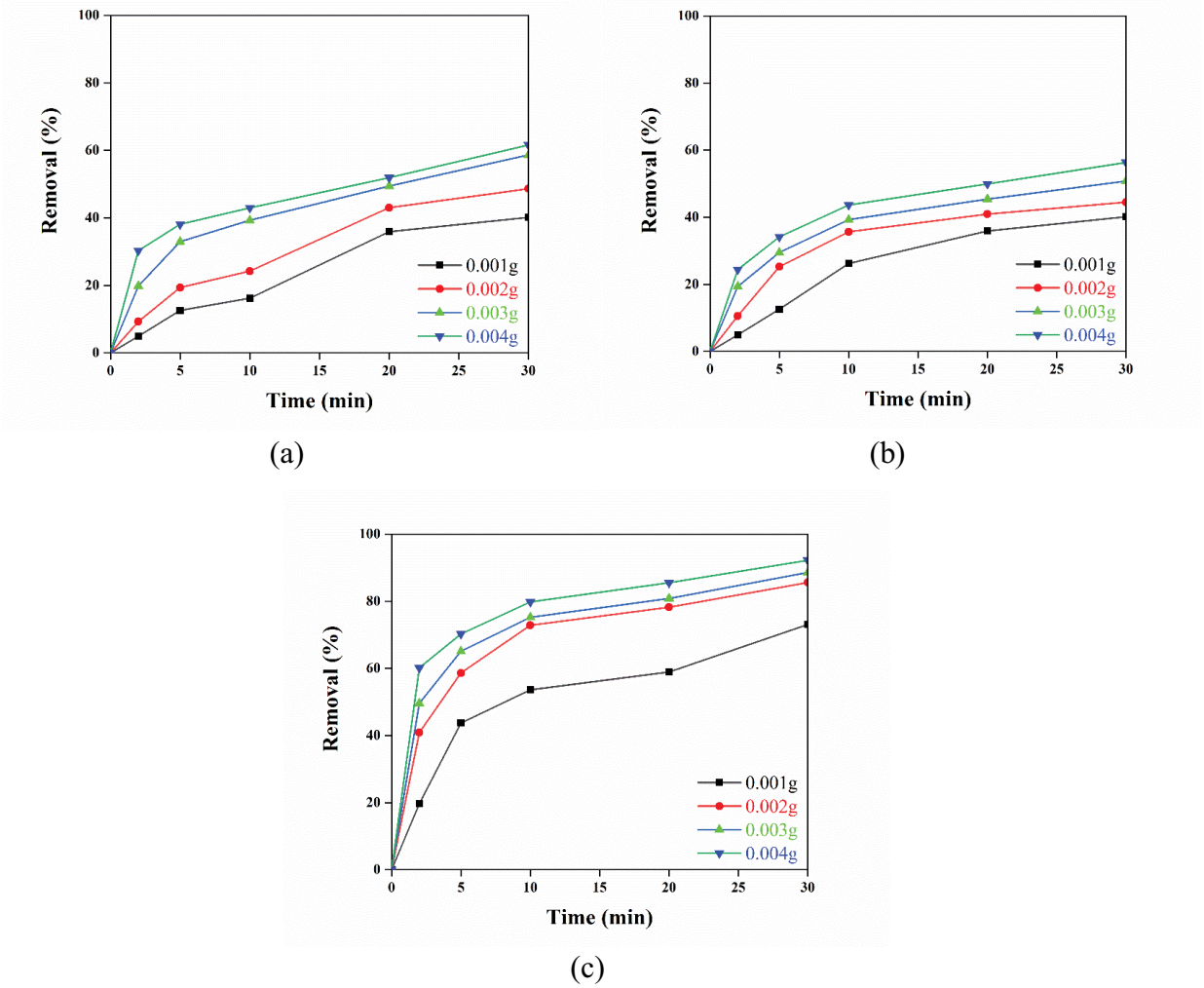

Fig. 6. Adsorbent dosage effect on dye removal (a) ZnO, (b) ZIF-8, and (c) ZnO-ZIF-8.

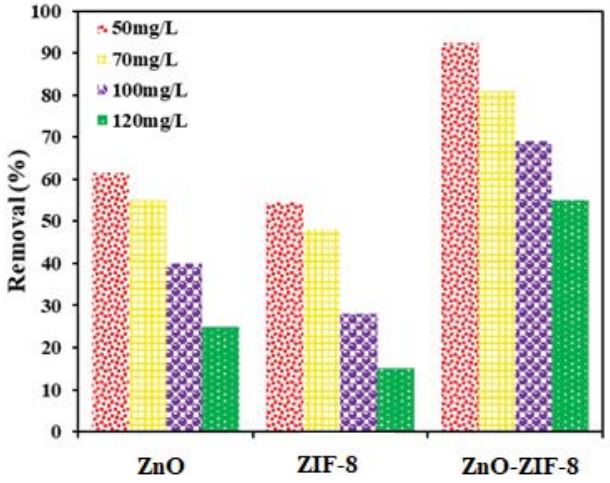

Fig. 7. Dye concentration effect on dye removal using ZnO, ZIF-8, and ZnO-ZIF-8.

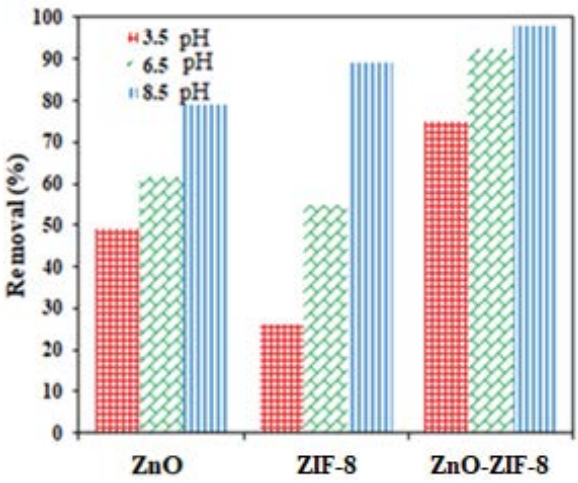

Fig. 8. Effect of pH on dye removal using ZnO, ZIF-8, and ZnO-ZIF-8.

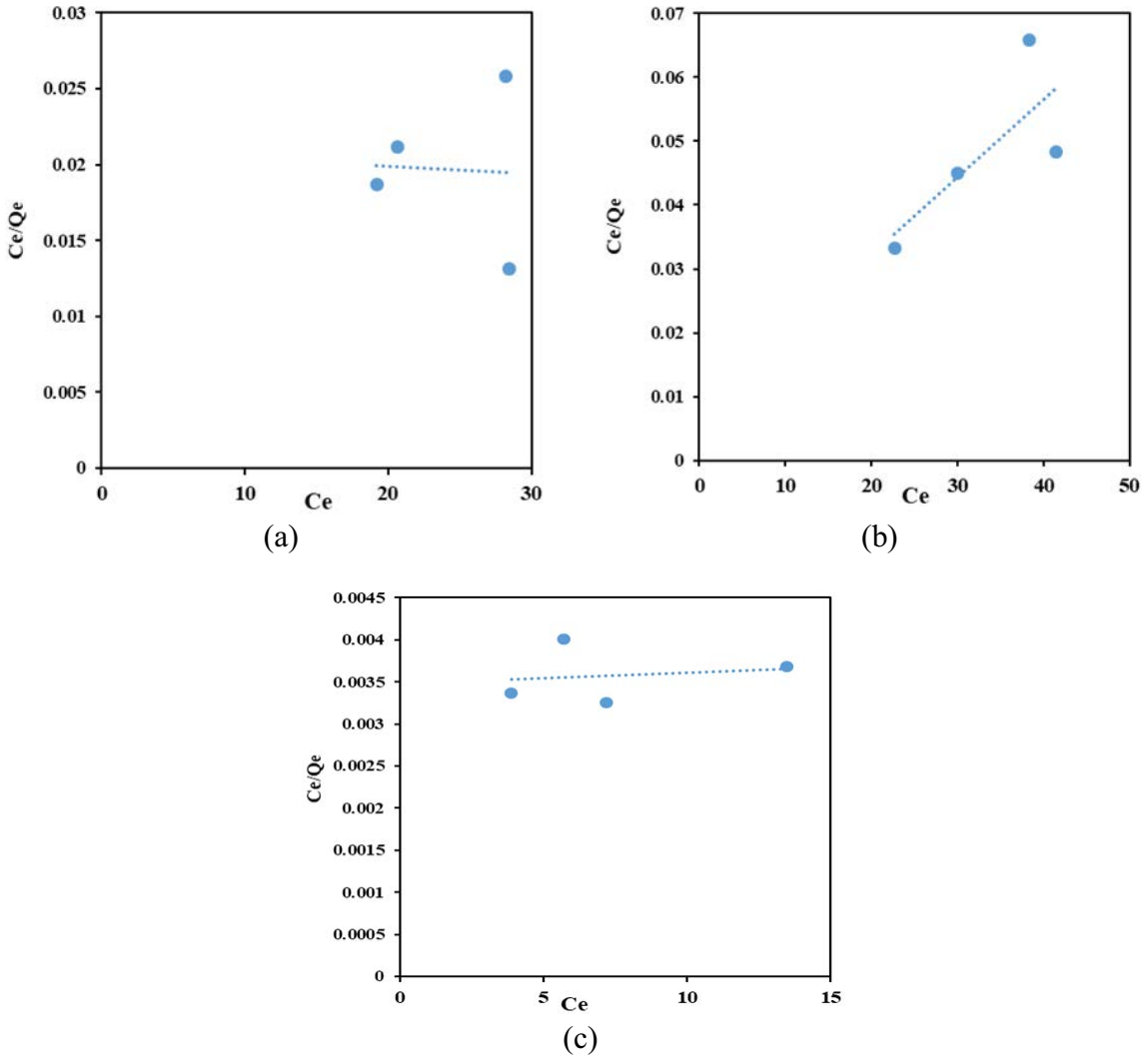

Fig. 9. Langmuir dye adsorption isotherm (a) ZnO, (b) ZIF-8, and (c) ZnO-ZIF-8.

ZnO-ZIF-8 = 92%), (pH 8.5: dye removal percentage for ZnO = 79%, ZIF-8 = 92%, and ZnO-ZIF-8 = 98%). Based on observations and experiments, the performance was better when pH was 8.5. It can be concluded that the adsorbent performance is dependent on the pH value.

3.2.5. Dye removal isotherm

The relationship between the amount of dye adsorbed onto the adsorbent and liquid phase concentration can be explained by isotherm. The Langmuir [39], Freundlich [42], and Temkin [23] isotherms are studied in our paper (Figs. 9–11). One of the isotherms that have successfully described many adsorption processes is the Langmuir isotherm. This isotherm can be used to describe the adsorption of dyes based on the Langmuir theory, according to which dedicated adsorption sites are responsible for the adsorption process. q_e, C_e, K_L, and Q_0 are adsorbent capacity at equilibrium (mg/g), the equilibrium concentration of dye solution (mg/L), the Langmuir constant (L/mg), and the maximum adsorbent capacity (mg/g), respectively. The experimental data were also compared with the Freundlich isotherm. K_F is the adsorption capacity per unit concentration, and $1/n$ is the adsorption intensity. $1/n$ values indicate the type of isotherm to be irreversible ($1/n = 0$), favorable ($0 < 1/n < 1$), and unfavorable ($1/n > 1$). The Temkin isotherm precisely examines the interaction of the adsorbent species. According to this isotherm, the heat of adsorption of all molecules on the adsorbent surface decreases linearly with the amount of surface coverage due to the adsorbent–adsorbent interactions. K_T and B_1 are the Temkin constants. Q_0 and K_L (constants of the Langmuir isotherm), K_F and $1/n$ (constants of the Freundlich isotherm), and K_T and B_1 (constants of Temkin isotherm) are shown in Table 1. Based on the data shown in Table 1, the best and most appropriate isotherm for the composite is the Freundlich model. Moreover, Table 2 compares the results of this study with those of the literature.

3.2.6. Binary system dye removal

Colored wastewater can have two or more dyes with different chemical structures. Dyes may interfere with each other causing a negative impact on the adsorption

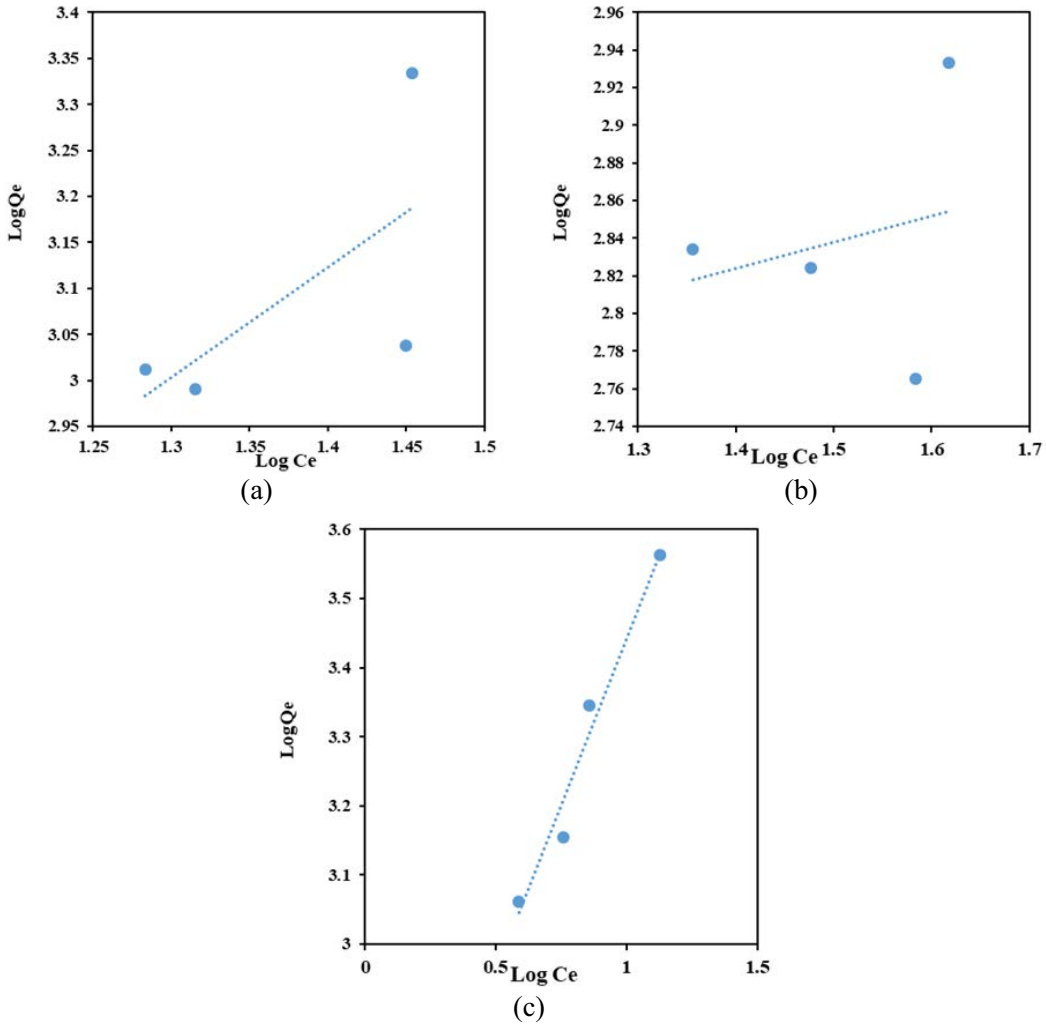

Fig. 10. Freundlich dye adsorption isotherm (a) ZnO, (b) ZIF-8, and (c) ZnO-ZIF-8.

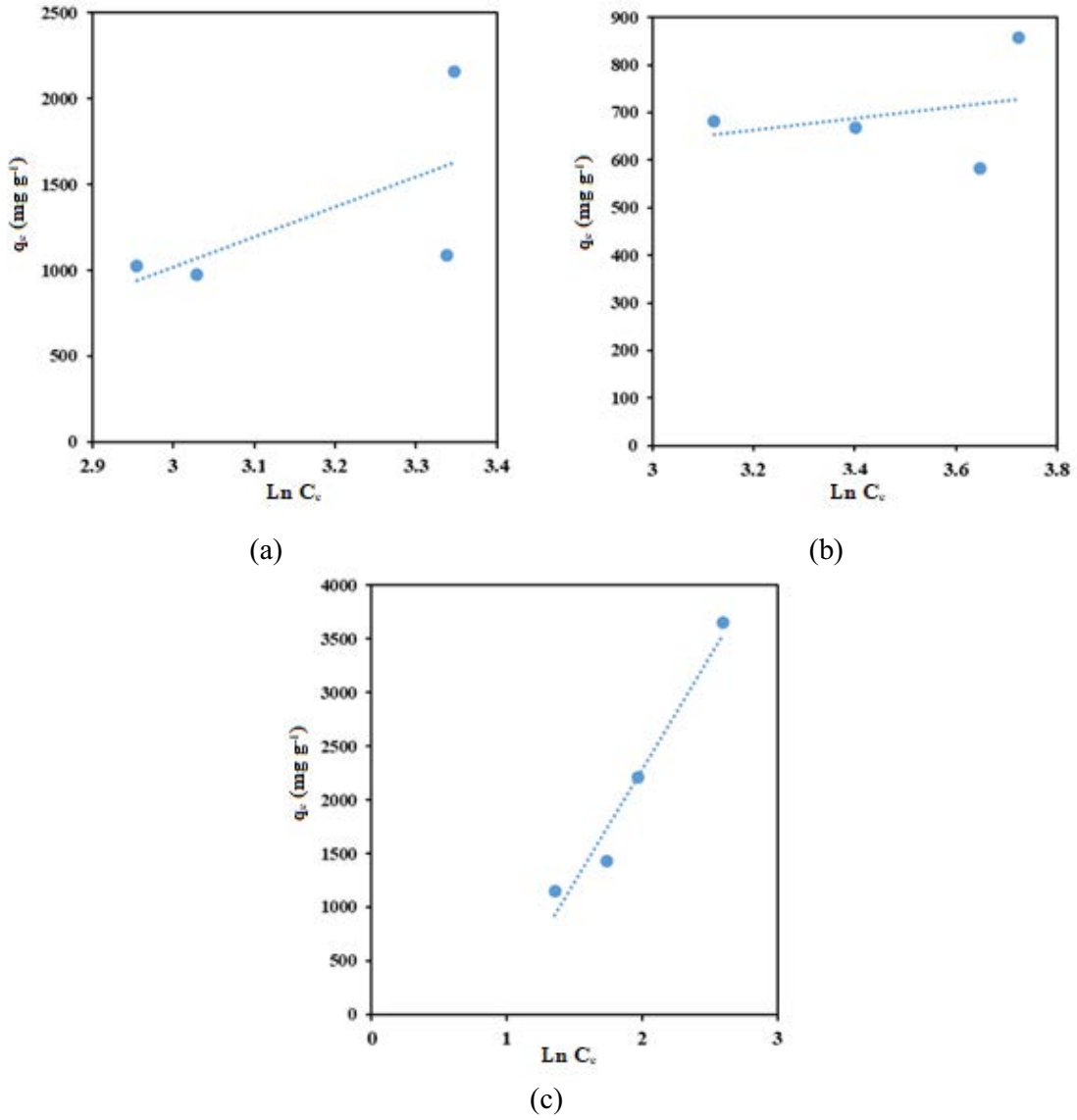

Fig. 11. Temkin dye adsorption isotherm (a) ZnO, (b) ZIF-8, and (c) ZnO-ZIF-8.

Table 1
Constants of adsorption isotherms of the synthesized materials

Adsorbent	Langmuir $C_e/q_e = 1/K_LQ_0 + C_e/Q_0$			Freundlich $\log q_e = \log K_F + 1/n \log C_e$			Temkin $q_e = B_1 \ln K_T + B_1 \ln C_e$		
	MG								
	Q_0	K_L	R^2	K_F	$1/n$	R^2	K_T	B_1	R^2
ZnO	200	0.0024	0.0019	27.98	1.4470	0.4348	11.25	1,756	0.406
ZIF-8	833	0.1480	0.5700	424.52	0.1400	0.0564	8.76	123	0.085
ZnO-ZIF-8	1,000	0.0028	0.0289	299.92	0.9650	0.9676	2.50	1,934	0.950

process. To test this issue, we mixed two dyes for preparing a binary system containing MG and Rh-B. MG and Rh-B were added to 1,000 mL of water (pH 6.5). 0.004 g adsorbent was used. The results of the adsorption process are as follows: for MG dye removal percentage for ZnO = 60%, ZIF-8 = 55%, ZnO-ZIF-8 = 94%, and for Rh-B the percentage of dye removal for ZnO = 19%, ZIF-8 = 25%, and ZnO-ZIF-8 = 22% (Fig. 12). Based on the results of the experiments, it can be concluded that the adsorption of MG was not affected in a binary system.

Table 2
Comparison between the results of this study and those of the literature

Adsorbent	Dye	Absorption capacity (mg/g)	Dye concentration (mg/L)	Reference
Copper oxide nanoparticle loaded on activated carbon	Blue acid 129	65.36	20	[43]
Copper oxide–nickel oxide	Basic red 18	55	20	[44]
β-Nickel hydroxide	Basic blue 41	120.48	20	[45]
ZnO-ZIF-8	Malachite Green	1,152.89	50	Our study

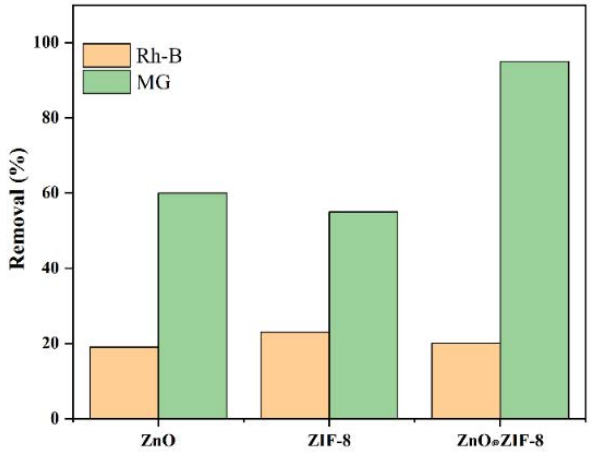

Fig. 12. Dye removal from binary systems.

4. Conclusion

This study investigated the performance of ZnO-ZIF-8 in dye (MG) adsorption from wastewater in the single and binary systems. After synthesizing materials and comparing the dye removal ability of ZnO, ZIF-8, and ZnO-ZIF-8 under similar operating conditions, it was found that combining these materials and preparing ZnO-ZIF-8 composite is a suitable method for increasing the adsorbent efficiency for removal of MG. The SEM, XRD, FT-IR, and zeta techniques were employed to study the structure of the adsorbents. The influence of operating parameters, including adsorbent dosage, time, initial dye concentration, and pH of the solution, was assessed. Equilibrium data were fitted by the Freundlich isotherm model. Finally, it can be concluded that ZnO-ZIF-8 composite had a high adsorption capacity for dye removal from colored wastewater.

References

[1] N.M. Mahmoodi, J. Abdi, M. Oveisi, M.A. Asli, M. Vossoughi, Metal-organic framework (MIL-100 (Fe)): synthesis, detailed photocatalytic dye degradation ability in colored textile wastewater and recycling, Mater. Res. Bull., 100 (2018) 357–366.
[2] N.M. Mahmoodi, N.Y. Limaee, M. Arami, S. Borhany, M. Mohammad-Taheri, Nanophotocatalysis using nanoparticles of titania: mineralization and finite element modelling of solophenyl dye decolorization, J. Photochem. Photobiol., A, 189 (2007) 1–6.
[3] A. Naseri, M. Samadi, N.M. Mahmoodi, A. Pourjavadi, H. Mehdipour, A.Z. Moshfegh, Tuning composition of electrospun ZnO/CuO nanofibers: toward controllable and efficient solar photocatalytic degradation of organic pollutants, J. Phys. Chem. C, 121 (2017) 3327–3338.
[4] [4] B. Hayati, A. Maleki, F. Najafi, H. Daraei, F. Gharibi, G. McKay, Adsorption of Pb^{2+}, Ni^{2+}, Cu^{2+}, Co^{2+} metal ions from aqueous solution by PPI/SiO_2 as new high-performance adsorbent: preparation, characterization, isotherm, kinetic, thermodynamic studies, J. Mol. Liq. 237 (2017) 428–436.
[5] N.M. Mahmoodi, Manganese ferrite nanoparticle: synthesis, characterization, and photocatalytic dye degradation ability, Desal. Water Treat., 53 (2015) 84–90.
[6] B. Hayati, N.M. Mahmoodi, A. Maleki, Dendrimer–titania nanocomposite: synthesis and dye-removal capacity, Res. Chem. Int., 41 (2015) 3743–3757.
[7] N.M. Mahmoodi, Dendrimer functionalized nanoarchitecture: synthesis and binary system dye removal, J. Taiwan Inst. Chem. Eng., 45 (2014) 2008–2020.
[8] O. Tavakoli, V. Goodarzi, M.R. Saeb, N.M. Mahmoodi, R. Borja, Competitive removal of heavy metal ions from squid oil under isothermal condition by CR11 chelate ion exchanger, J. Hazard. Mater., 334 (2017) 256–266.
[9] N.M. Mahmoodi, Nickel ferrite nanoparticle: synthesis, modification by surfactant and dye removal ability, Water Air Soil Pollut., 224 (2013) 1419, doi: 10.1007/s11270-012-1419-7.
[10] S.M. Ibrahim, A.A. Badawy, H.A. Essawy, Improvement of dyes removal from aqueous solution by nanosized cobalt ferrite treated with humic acid during coprecipitation, J. Nanostruct. Chem., 9 (2019) 281–298.
[11] N.M. Mahmoodi, J. Abdi, D. Bastani, Direct dyes removal using modified magnetic ferrite nanoparticle, J. Environ. Health Sci. Eng., 12 (2014) 96, doi: 10.1186/2052-336X-12-96.
[12] A. Almasian, M.E. Olya, N.M. Mahmoodi, Synthesis of polyacrylonitrile/polyamidoamine composite nanofibers using electrospinning technique and their dye removal capacity, J. Taiwan Inst. Chem. Eng., 49 (2015) 119–128
[13] N.M. Mahmoodi, B. Hayati, H. Bahrami, M. Arami, Dye adsorption and desorption properties of Mentha pulegium in single and binary systems, J. Appl. Polym. Sci., 122 (2011) 1489–1499.
[14] E. Haque, J.W. Jun, S.H. Jhung, Adsorptive removal of methyl orange and methylene blue from aqueous solution with a metal-organic framework material, iron terephthalate (MOF-235), J. Hazard. Mater., 185 (2011) 507–511.
[15] N.A. Khan, Z. Hasan, S.H. Jhung, Adsorptive removal of hazardous materials using metal-organic frameworks (MOFs): a review, J. Hazard. Mater., 244 (2013) 444–456.
[16] G. Ren, Z. Li, W. Yang, M. Faheem, J. Xing, X. Zou, Q. Pan, G. Zhu, Y. Du, ZnO@ZIF-8 core-shell microspheres for improved ethanol gas sensing, Sens. Actuators, B, 284 (2019) 421–427.
[17] C. Yang, L. Yu, R. Chen, J. Cheng, Y. Chen, Y. Hu, Congo red adsorption on metal-organic frameworks, MIL-101 and ZIF-8: kinetics, isotherm and thermodynamic studies, 94 (2017) 211–221.
[18] F. Xiao, J. Cheng, X. Fan, C. Yan, Y. Hu, Adsorptive removal of the hazardous anionic dye Congo red and mechanistic study of ZIF-8, Desal. Water Treat., 101 (2018) 291–300.
[19] R. Gong, Y. Jin, F. Chen, J. Chen, Z. Liu, Enhanced malachite green removal from aqueous solution by citric acid modified rice straw, J. Hazard. Mater., 137 (2006) 865–870.

[20] S.D. Khattri, M.K. Singh, Removal of malachite green from dye wastewater using neem sawdust by adsorption, J. Hazard. Mater., 167 (2009) 1089–1094.
[21] A. Verma, S. Thakur, G. Mamba, R.K. Gupta, P. Thakur, V.K. Thakur, Graphite modified sodium alginate hydrogel composite for efficient removal of malachite green dye, Int. J. Biol. Macromol., 148 (2020) 1130–1139.
[22] A. Malik, M. Nath, Multicore–shell nanocomposite formed by encapsulation of WO_3 in zeolitic imidazolate framework (ZIF-8): as an efficient photocatalyst, J. Environ. Chem. Eng., 7 (2019) 103401, doi: 10.1016/j.jece.2019.103401.
[23] N.M. Mahmoodi, H. Chamani, H.-R. Kariminia, Functionalized copper oxide–zinc oxide nanocomposite: synthesis and genetic programming model of dye adsorption, Desal. Water Treat., 57 (2016) 18755–18769.
[24] J.I. Goldstein, D.E. Newbury, J.R. Michael, N.W.M. Ritchie, J.H.J. Scott, D.C. Joy, Scanning Electron Microscopy and X-Ray Microanalysis, Springer, Switzerland, 2017.
[25] E.L. Bustamante, J.L. Fernández, J.M. Zamaro, Influence of the solvent in the synthesis of zeolitic imidazolate framework-8 (ZIF-8) nanocrystals at room temperature, J. Colloid Interface Sci., 424 (2014) 37–43.
[26] X. He, D.-P. Yang, X. Zhang, M. Liu, Z. Kang, C. Lin, N. Jia, R. Luque, Waste eggshell membrane-templated CuO-ZnO nanocomposites with enhanced adsorption, catalysis and antibacterial properties for water purification, Chem. Eng. J., 369 (2019) 621–633.
[27] G.N.S. Vijayakumar, S. Devashankar, M. Rathnakumari, P. Sureshkumar, Synthesis of electrospun ZnO/CuO nanocomposite fibers and their dielectric and non-linear optic studies, J. Alloys Compd., 507 (2010) 225–229.
[28] Y. Xie, R. Xing, Q. Li, L. Xu, H. Song, Three-dimensional ordered ZnO–CuO inverse opals toward low concentration acetone detection for exhaled breath sensing, Sens. Actuators B, 211 (2015) 255–262.
[29] X.-C. Huang, Y.-Y. Lin, J.-P. Zhang, X.-M. Chen, Ligand-directed strategy for zeolite-type metal–organic frameworks: zinc(II) imidazolates with unusual zeolitic topologies, Angew. Chem. Int. Ed., 45 (2006) 1557–1559.
[30] S. Gadipelli, T. Zhao, S.A. Shevlin, Z. Guo, Switching effective oxygen reduction and evolution performance by controlled graphitization of a cobalt–nitrogen–carbon framework system, Energy Environ. Sci., 9 (2016) 1661–1667.
[31] E.E. Sann, Y. Pan, Z. Gao, S. Zhan, F. Xia, Highly hydrophobic ZIF-8 particles and application for oil-water separation, Sep. Purif. Technol., 206 (2018) 186–191.
[32] M. Oveisi, N.M. Mahmoodi, M. Alinia Asli, Halogen lamp activated nanocomposites as nanoporous photocatalysts: synthesis, characterization, and pollutant degradation mechanism, J. Mol. Liq., 281 (2019) 389–400.
[33] Y. Hu, H. Kazemian, S. Rohani, Y. Huang, Y. Song, *In situ* high pressure study of ZIF-8 by FTIR spectroscopy, Chem. Commun., 47 (2011) 12694–12696.
[34] J.-B. Huo, L. Xu, J.-C.E. Yang, H.-J. Cui, B. Yuan, M.-L. Fu, Magnetic responsive Fe_3O_4-ZIF-8 core-shell composites for efficient removal of As(III) from water, Colloids Surf., A, 539 (2018) 59–68.
[35] N. Li, L. Zhou, X. Jin, G. Owens, Z. Chen, Simultaneous removal of tetracycline and oxytetracycline antibiotics from wastewater using a ZIF-8 metal organic-framework, J. Hazard. Mater., 366 (2019) 563–572.
[36] M. He, J. Yao, Q. Liu, K. Wang, F. Chen, H. Wang, Facile synthesis of zeolitic imidazolate framework-8 from a concentrated aqueous solution, Microporous Mesoporous Mater., 184 (2014) 55–60.
[37] T. Hurma, Effect of boron doping concentration on structural optical electrical properties of nanostructured ZnO films, J. Mol. Struct., 1189 (2019) 1–7.
[38] H. Tian, H. Fan, M. Li, L. Ma, Zeolitic imidazolate framework coated ZnO nanorods as molecular sieving to improve the selectivity of formaldehyde gas sensor, ACS Sens., 1 (2016) 243–250.
[39] G. Crini, P.-M. Badot, Application of chitosan, a natural aminopolysaccharide, for dye removal from aqueous solutions by adsorption processes using batch studies: a review of recent literature, Prog. Polym. Sci., 33 (2008) 399–447.
[40] N.M. Mahmoodi, M. Oveisi, M. Bakhtiari, B. Hayati, A.A. Shekarchi, A. Bagheri, S. Rahimi, Environmentally friendly ultrasound-assisted synthesis of magnetic zeolitic imidazolate framework-Graphene oxide nanocomposites and pollutant removal from water, J. Mol. Liq., 282 (2019) 115–130.
[41] N.M. Mahmoodi, J. Abdi, Surface modified cobalt ferrite nanoparticles with cationic surfactant: synthesis, multicomponent dye removal modeling and selectivity analysis, Prog. Color Colorants Coat., 12 (2019) 163–177.
[42] S.P. Mishra, M.R. Ghosh, Use of silver impregnated activated carbon (SAC) for Cr(VI) removal, J. Environ. Chem. Eng., 8 (2020) 103641, doi: 10.1016/j.jece.2019.103641.
[43] F. Nekouei, S. Nekouei, I. Tyagi, V.K. Gupta, Kinetic, thermodynamic and isotherm studies for acid blue 129 removal from liquids using copper oxide nanoparticle-modified activated carbon as a novel adsorbent, J. Mol. Liq., 201 (2015) 124–133.
[44] N.M. Mahmoodi, Z. Hosseinabadi-Farahani, F. Bagherpour, M.R. Khoshrou, H. Chamani, F. Forouzeshfar, Synthesis of CuO-NiO nanocomposite and dye adsorption modeling using artificial neural network, Desal. Water Treat., 57 (2016) 17220–17229.
[45] N.M. Mahmoodi, Z. Hosseinabadi-Farahani, H. Chamani, Synthesis of nanostructured adsorbent and dye adsorption modeling by an intelligent model for multicomponent systems, Korean J. Chem. Eng., 33 (2016) 902–913.